PNAS RESEARCH ARTICLE | BIOCHEMISTRY

Refining the mechanism of heme acquisition from free hemoglobin by *Staphylococcus aureus* IsdH

Valeria Buoli Comani[a,b], Omar De Bei[c,1], Giulia Paris[d], Marialaura Marchetti[c], Francesca Pancrazi[e], Barbara Campanini[a,b], Luca Ronda[b,c,f], Ben F. Luisi[d], Serena Faggiano[a,f], Anna Rita Bizzarri[e], and Stefano Bettati[b,c,f,1]

Affiliations are included on p. 10.

Edited by Catherine L. Drennan, Massachusetts Institute of Technology, Cambridge, MA; received January 17, 2026; accepted April 8, 2026

Staphylococcus aureus **is a human pathogen whose virulence depends on iron acquisition. The bacterium expresses the hemophores IsdB and IsdH that enable heme capture from host hemoglobin (Hb). Unlike IsdB, IsdH can bind both free Hb and Hb:haptoglobin (Hb:Hp) complexes. Here, we present a comprehensive structural analysis of full-length IsdH in complex with free Hb, overcoming the limitations of previous studies based on truncated IsdH constructs. Cryo-EM revealed a previously unobserved oligomeric state and a unique binding pose of the N-terminal Hb-binding domain, likely representing the initial step of Hb engagement. Time-resolved and single-molecule force spectroscopy experiments delineated the sequential steps and mechanical aspects of Hb binding and heme extraction. Together, these findings provide an integrated structural and functional view of the IsdH–Hb interaction in the absence of Hp, as may occur during hemolysis, and offer insights into *S. aureus* heme scavenging and potential avenues for therapeutic inhibition.**

Staphylococcus aureus | hemoglobin | IsdH | AMR | iron acquisition

Staphylococcus aureus is a human pathogen responsible for skin and soft tissue infections as well as for life-threatening conditions such as sepsis and endocarditis (1). The ability of this bacterium to cause diseases relies on its capacity to acquire essential nutrients from the host environment (2, 3). Iron, a critical cofactor for numerous metabolic and enzymatic processes, is highly sequestered in vertebrates, primarily within the heme prosthetic group of host hemoproteins like hemoglobin (Hb) and myoglobin (4). To overcome this nutritional challenge, *S. aureus* has evolved a sophisticated and highly efficient iron-regulated surface determinant (Isd) system to retrieve iron from its most abundant circulating source, Hb (5–7).

The Isd system is a multiprotein relay pathway that starts with cell wall-anchored surface proteins, IsdB and IsdH, which serve as the initial receptors for host Hb (8). Heme is then sequentially transferred across the bacterial cell wall *via* the intermediate proteins IsdA and IsdC to the membrane transporter IsdE, and finally into the cytoplasm for degradation by the heme oxygenases IsdG and IsdI, which release the iron ion for bacterial use. While IsdB is considered the primary Hb receptor and is critical for pathogenesis in murine infection models (9, 10), IsdH may play a distinct, possibly complementary role in heme acquisition (11, 12). The coexistence of two apparently redundant hemophores likely reflects the evolutionary pressure exerted by host–pathogen interactions.

In this competitive interplay, the host exploits the serum protein haptoglobin (Hp) (13), whose primary role is to bind free oxidized Hb with high affinity, thereby limiting not only Hb toxicity but also bacterial access to heme. IsdH has been proposed to interact with the Hb:Hp complex and possibly extract the heme from the complex (14, 15)—a capability not attributed to IsdB (16). At the same time, IsdH has also been shown to bind Hb and extract heme with efficiency comparable to IsdB (17, 18). This potential dual functional specialization of IsdH may thus represent a bacterial adaptation to circumvent host defense mechanisms, underscoring a plausible facet of the ongoing coevolutionary arms race for the iron nutrient.

The functional distinction between IsdB and IsdH is mirrored in their structural composition. Both proteins rely on NEAr-iron Transporter (NEAT, N) domains to interact with Hb and heme (12, 19), yet differ in the number and spatial arrangement of these domains. IsdB possesses two NEAT domains, $IsdB^{N1}$ for Hb binding and $IsdB^{N2}$ for heme binding and extraction (20). IsdH, in contrast, has three NEAT domains—$IsdH^{N1}$, $IsdH^{N2}$, and $IsdH^{N3}$—linked by flexible linker regions (12, 21). The first two NEATs mediate Hb binding, whereas the third extracts heme; while Linker1 remains uncharacterized, Linker2 consists of three α-helices.

Significance

Bacterial pathogens must acquire essential nutrients from the human host to survive and cause infection. One of the most important is iron, which in our bloodstream is sequestered inside hemoglobin. *Staphylococcus aureus* overcomes this barrier using surface proteins that capture hemoglobin and extract its heme cofactor. Until now, one of these proteins, IsdH, has mainly been studied in a truncated form, potentially masking important aspects of its biological function. Here, we present the structure of full-length IsdH and identify a previously unrecognized mechanism by which its architecture engages hemoglobin and enables heme release. Integrating structural, kinetic, and single-molecule approaches, this work refines our understanding of host–pathogen interactions in iron acquisition and highlights opportunities for targeting this pathway in antimicrobial strategies.

Author contributions: O.D.B., M.M., B.C., L.R., B.F.L., S.F., A.R.B., and S.B. designed research; V.B.C., O.D.B., G.P., F.P., and A.R.B. performed research; V.B.C., O.D.B., and F.P. analyzed data; A.R.B. and S.B. funding acquisition; S.B. project administration; and V.B.C., O.D.B., G.P., M.M., F.P., B.C., L.R., B.F.L., S.F., A.R.B., and S.B. wrote the paper.

The authors declare no competing interest.

This article is a PNAS Direct Submission.

Copyright © 2026 the Author(s). Published by PNAS. This article is distributed under Creative Commons Attribution-NonCommercial-NoDerivatives License 4.0 (CC BY-NC-ND).

[1]To whom correspondence may be addressed. Email: omar.debei@unipr.it or stefano.bettati@unipr.it.

This article contains supporting information online at https://www.pnas.org/lookup/suppl/doi:10.1073/pnas.2601134123/-/DCSupplemental.

Published May 11, 2026.

Downloaded from https://www.pnas.org by UNIVERSITA DEGLI STUDI DI PARMA on May 11, 2026 from IP address 160.78.140.1.

To date, structural studies on IsdH have relied on truncated constructs (15, 18, 22, 23). Similarly, most functional studies have largely followed the same approach (17, 18, 24), with only limited investigations on the full-length protein (25–27), for which structure–function relationship studies remain incomplete. This strategy is experimentally convenient, but it does not fully capture the native behavior of the protein. The architecture of the full-length protein, which includes an additional NEAT domain and an extended flexible region, inherently complicates its expression and analysis. Nevertheless, only the full-length IsdH, comprising all three NEAT domains and their natural linkers, reflects the physiologically relevant context in which Hb heme scavenging occurs.

The present study addresses this limitation by providing comprehensive structural and functional characterization of the full-length wild-type IsdH protein in complex with free Hb. This interaction reflects a physiologically likely relevant condition that may occur during severe hemolysis induced by *S. aureus* hemolysins, when Hp becomes depleted and can no longer effectively sequester all released Hb (28). Using a combination of biophysical and structural techniques, including size-exclusion chromatography, cryoelectron microscopy (cryo-EM), binding affinity assays, and kinetic analysis, we investigated how IsdH engages Hb and extracts heme. Our findings reveal a specific binding mode and a defined stoichiometric requirement for heme extraction, providing insights into the molecular mechanisms governing IsdH function. Together, these results refine our understanding of IsdH as a key component of the *S. aureus* heme acquisition machinery.

Results

Biochemical and Structural Characterization of Full-Length IsdH Interaction with Hb. We expressed and purified full-length *S. aureus* IsdH, which is composed of three domains separated by two linker regions. The size and distribution of IsdH:Hb complexes were initially analyzed by size-exclusion chromatography coupled with light scattering (SEC-LS). To trap the early interaction between the two proteins (i.e., the preextraction complex), we used oxyHb (oxygen-bound Hb, with heme iron in the Fe^{2+} reduced state), which is resistant to heme removal. Single proteins were first analyzed to establish references (Fig. 1 *A* and *B*). The molecular weights (MWs) determined by SEC-LS were in agreement with the theoretical values (Table 1). At the concentrations used, IsdH was monomeric, and Hb formed a mixture of dimers and tetramers.

The presence of two Hb-binding domains in IsdH raises the question of the component stoichiometry. Using an initial AlphaFold prediction, we identified the complex consisting of one IsdH receptor per Hb dimer as the most probable assembly (*SI Appendix*, Fig. S1 *A* and *B*). Therefore, SEC-LS experiments on the preextraction complex were performed by mixing IsdH with oxyHb under conditions favoring this stoichiometry. This mixture yielded a single peak that eluted with an apparent MW of 98.7 kDa, consistent with one IsdH molecule bound to a Hb dimer. This complex is hereafter referred to as 1IsdH:Hb_{dim} (Fig. 1*C* and Table 1). The delayed elution of the complex compared to free IsdH indicates a more compact conformation of the hemophore upon Hb binding. Given that IsdH contains a flexible linker between its NEAT1 and NEAT2 domains (i.e., Linker1), it is plausible that complex formation stabilizes a condensed arrangement of these domains, resulting in a reduced hydrodynamic radius. To further validate the identified stoichiometry, a mixture containing a higher proportion of IsdH relative to oxyHb was analyzed, corresponding to two IsdH molecules per Hb dimer (Fig. 1*D*). Two peaks were observed in the chromatogram, with apparent MWs consistent with free IsdH and 1IsdH:Hb_{dim} complex, respectively (Table 1). These data confirm the binding of a single IsdH molecule to a Hb dimer.

To complement the biochemical analysis and obtain structural insights, we performed cryo-EM on 1IsdH:Hb_{dim} complex as isolated by SEC-LS. HbCO (i.e., carbon monoxide-bound Hb) was chosen instead of oxyHb due to its greater resistance to oxidation under sample preparation conditions (18, 29). Single-particle analysis (SPA) yielded a reconstruction at 3.14 Å for the dominant species in the sample (Fig. 1*E* and *SI Appendix*, Fig. S2 and Table S1), revealing a Hb dimer bound by a single IsdH receptor, in full agreement with the stoichiometry inferred from SEC-LS data. The cryo-EM reveals that the NEAT2-Linker2-NEAT3 region of IsdH engages the α-chain of Hb, while the NEAT1 domain unexpectedly binds a distinct pocket at the Hb dimer–dimer interface; together, the three domains form a dense network of intermolecular contacts (*SI Appendix*, Table S2 and Fig. S3). This architecture markedly deviates from the AlphaFold prediction (*SI Appendix*, Fig. S1*A*)—which placed NEAT2-Linker2-NEAT3 on the β-chains and NEAT1 on the α-chains of Hb—as well as from previously reported structural and biochemical data on isolated IsdH fragments (14, 23, 30). Interestingly, while the binding interfaces diverge from the predicted model, Linker1 connecting NEAT1 and NEAT2 behaves as anticipated: it is not resolved in the cryo-EM map, suggesting it remains flexible and unstructured, in agreement with the AlphaFold prediction.

Cryo-EM Reveals the Binding Mode of Full-Length IsdH on Free Hb. While the binding of the NEAT2–NEAT3 region to the α-chains is consistent with previous reports and shows largely overlapping contacts with published structures (*SI Appendix*, Table S2), the cryo-EM reconstruction of the IsdH:HbCO complex revealed an unexpected binding pose for the NEAT1 domain, which occupies a previously unrecognized pocket at the dimer–dimer interface of Hb (Fig. 1*E*). The observation appears to differ from previous studies, which described $IsdH^{N1}$ as a Hb-binding domain, like $IsdH^{N2}$, displaying selective recognition of the A/E helices of Hb α-chains (23, 30). This discrepancy might arise because in our model the α-chain is already engaged by the NEAT2-Linker2-NEAT3 portion, while for the previously reported structures isolated NEAT domains were used; such interactions would have been then unrestricted, allowing NEAT1 to bind regions that in the full-length protein are occupied by NEAT2. Notably, the available NEAT1:Hb crystal structure [PDB ID 3SZK (30)]—although showing NEAT1 in a different orientation—is consistent with our model when contacting neighbors in the crystal lattice are considered, supporting the structural plausibility of the NEAT1 position observed in our reconstruction (*SI Appendix*, Fig. S4).

A minor population of particles (<5,000) corresponding to a larger complex designated 1IsdH:2Hb_{dim} was identified. Although the map resolution was limited to 7.29 Å, it was sufficient for a reliable flexible fitting of a model (Fig. 1*F* and *SI Appendix*, Fig. S2). In this assembly, the canonical 1IsdH:Hb_{dim} complex observed at high resolution is still preserved, with NEAT2 and NEAT3 bound to the α-chain and NEAT1 positioned at the Hb dimer–dimer interface; additionally, NEAT1 also engages the α-chains of a second Hb dimer, demonstrating its selective recognition of α-chains in agreement with earlier reports (23, 30). These data provide clear structural evidence of NEAT1 dual binding capability.

To investigate whether the latent information within AI models could encode a binding mode similar to that observed for NEAT1, AlphaFold3 predictions were performed using an Hb dimer in the presence of either three $IsdH^{N1}$ or three $IsdH^{N2}$ domains (*SI Appendix*, Fig. S1 *C* and *D*). None of the generated models

Downloaded from https://www.pnas.org by UNIVERSITA DEGLI STUDI DI PARMA on May 11, 2026 from IP address 160.78.140.1.

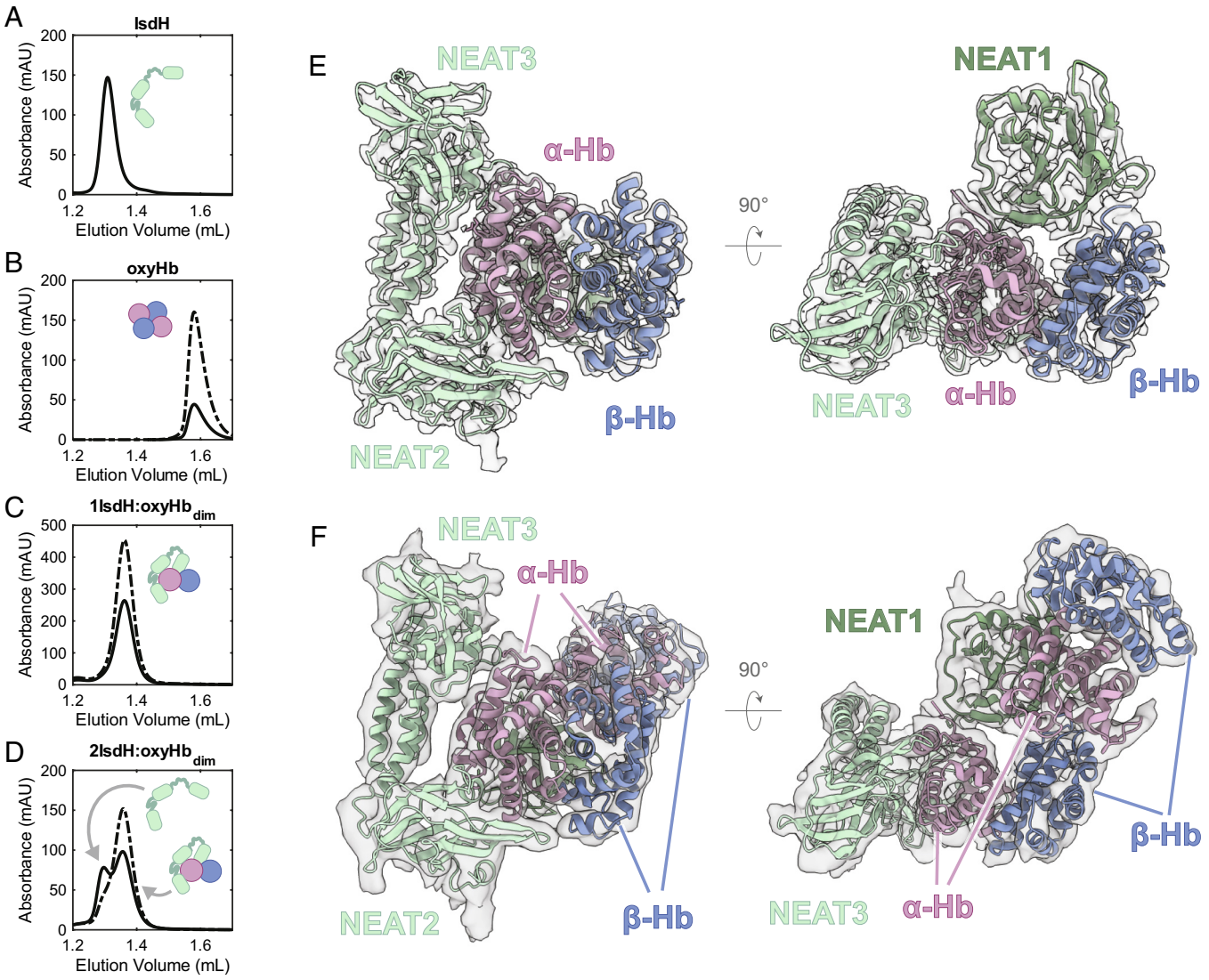


Fig. 1. Characterization of the IsdH:Hb preextraction complex. (*A–D*) SEC analysis of IsdH:oxyHb complexes at different stoichiometries, where Hb concentration is expressed on a dimer basis. Elution profiles were monitored at 280 nm (solid lines) and at 415 nm (dashed lines) and plotted against elution volume. (*A*) IsdH alone (18.25 μM); (*B*) oxyHb alone (9.12 μM); (*C*) 1 IsdH per $oxyHb_{dim}$ (18.25 μM: 18.25 μM); (*D*) 2 IsdH per $oxyHb_{dim}$ (18.25 μM: 9.12 μM). All experiments were performed in duplicate (n = 2), and the calculated MWs are reported in Table 1. (*E*) Cryo-EM map of the IsdH:Hb_{dim} complex (EMDB ID EMD-55389, shown in semi-transparent) with the refined model fitted (PDB ID 9SZW); a detailed view of the highlighted interaction interfaces is provided in *SI Appendix*, Fig. S3. (*F*) Cryo-EM map of the IsdH:$2Hb_{dim}$ complex (EMDB ID EMD-55478, shown in semi-transparent) with the relative model fitted (available on Figshare https://figshare.com/10.6084/m9.figshare.30751553). Color code: α-Hb in pink, β-Hb in blue, $IsdH^{N2N3}$ in light green and $IsdH^{N1}$ in dark green.

reproduced this configuration, indicating that the interaction geometry obtained using cryo-EM was not captured by current predictive models.

Beyond representing a previously unobserved binding pose, NEAT1 bound at the dimer–dimer interface of Hb bears a clear resemblance to the binding mode described for Hp in the Hb:Hp complex. To further investigate this similarity, we compared NEAT1–Hb binding with that of Hp in the recently reported Hb:Hp:CD163 model [PDB ID 9HEJ (31)] and in the Hb:Hp:$IsdH^{N2N3}$ complex [PDB ID 6TB2 (15)]. Analysis of buried surface area (BSA) in these complexes reveals that Hp engages a slightly larger BSA with the Hb dimer (over 2,900 $Å^2$) than NEAT1 (~2,200 $Å^2$) (*SI Appendix*, Table S3). For a more detailed analysis, we employed RING (https://ring.biocomputingup.it/) to identify all direct polar and nonpolar contacts between NEAT1 or Hp and the Hb dimer in the three models. To provide structural context and enhance interpretability, individual interactions were mapped onto the secondary structure elements of Hb, following the conventional topological nomenclature (32). The resulting heatmap (Fig. 2 *A* and *B*) shows that Hp exhibits a conserved interaction pattern across both complexes [i.e., PDB IDs 9HEJ (31) and 6TB2 (15)]. In contrast, NEAT1 establishes very few contacts with the α-chains, while its interactions with the β-chains differ markedly from those of Hp. Specifically, Hp contacts helices C and G and the FG loop, whereas NEAT1 interacts only weakly with helix C and the FG loop but engages extensively with the β-chain C-terminal region.

To estimate the binding affinity of NEAT1 for the Hb dimer–dimer interface, we employed PRODIGY [PROtein binDIng enerGY prediction (34)], a structure-based method that predicts binding free energy (ΔG) and dissociation constants (K_D) from interfacial contacts and physicochemical properties of the complex. The calculated parameters are reported in Table 2. Consistent with these predictions, the estimated affinities fall in the nanomolar range and correlate well with the experimental data (*SI Appendix*, Fig. S5*A*), which show measurable binding of NEAT1 to Hb (K_D metHb: 23.15 ± 7.16 nM; K_D oxyHb: 12.33 ± 4.08 nM). Notably, when the affinity of NEAT1 is estimated in complex with the α

Downloaded from https://www.pnas.org by UNIVERSITA DEGLI STUDI DI PARMA on May 11, 2026 from IP address 160.78.140.1.

Table 1. Summary of SEC-LS experiment to determine IsdH:Hb complex stoichiometry

Experiment condition	Measured MW (kDa)	Theoretical MW (kDa)	Inferred stoichiometry
IsdH alone	72.1 ± 0.8	~70	monomer
oxyHb alone	54.9 ± 2.2	~32/~64	dimer-tetramer mixture
metHb alone	51.8 ± 5.1	~32/~64	dimer-tetramer mixture
1 IsdH − 1 $oxyHb_{dim}$	101.2 ± 4.5	~102	$1IsdH:Hb_{dim}$
2 IsdH − 1 $oxyHb_{dim}$	80.2 ± 2.3 107.8 ± 6.2	~70 ~102	free IsdH + $1IsdH:Hb_{dim}$

subunits alone [PDB 3SZK (30)], the predicted value is markedly reduced (Table 2), indicating that the Hb dimer–dimer interface provides a more favorable binding environment. When considering Hp binding at the same Hb dimer–dimer interface [PDB 9HEJ (31)], the predicted affinity increases dramatically, reaching a K_D in the picomolar range, consistent with previously reported high-affinity Hb–Hp interaction (35). Taken together, these results indicate that NEAT1 binding to Hb does not occlude Hp binding site or compete with Hp. Consistent with this model, NEAT2–NEAT3 of IsdH can remain bound to the α-chains of Hb within the Hb:Hp complex, while NEAT1 could in principle engage a second Hb dimer associated with the alternate Hp protomer. This configuration is enabled by the extended and flexible linker connecting NEAT1 and NEAT2, which can bridge the two Hb dimers (*SI Appendix*, Fig. S4 *B* and *C*).

To assess the structural consequences of NEAT1 binding, we compared the Hb dimer structure [PDB ID 2DN1 (33)] with the cryo-EM model obtained in this study (Fig. 2*C*). Upon

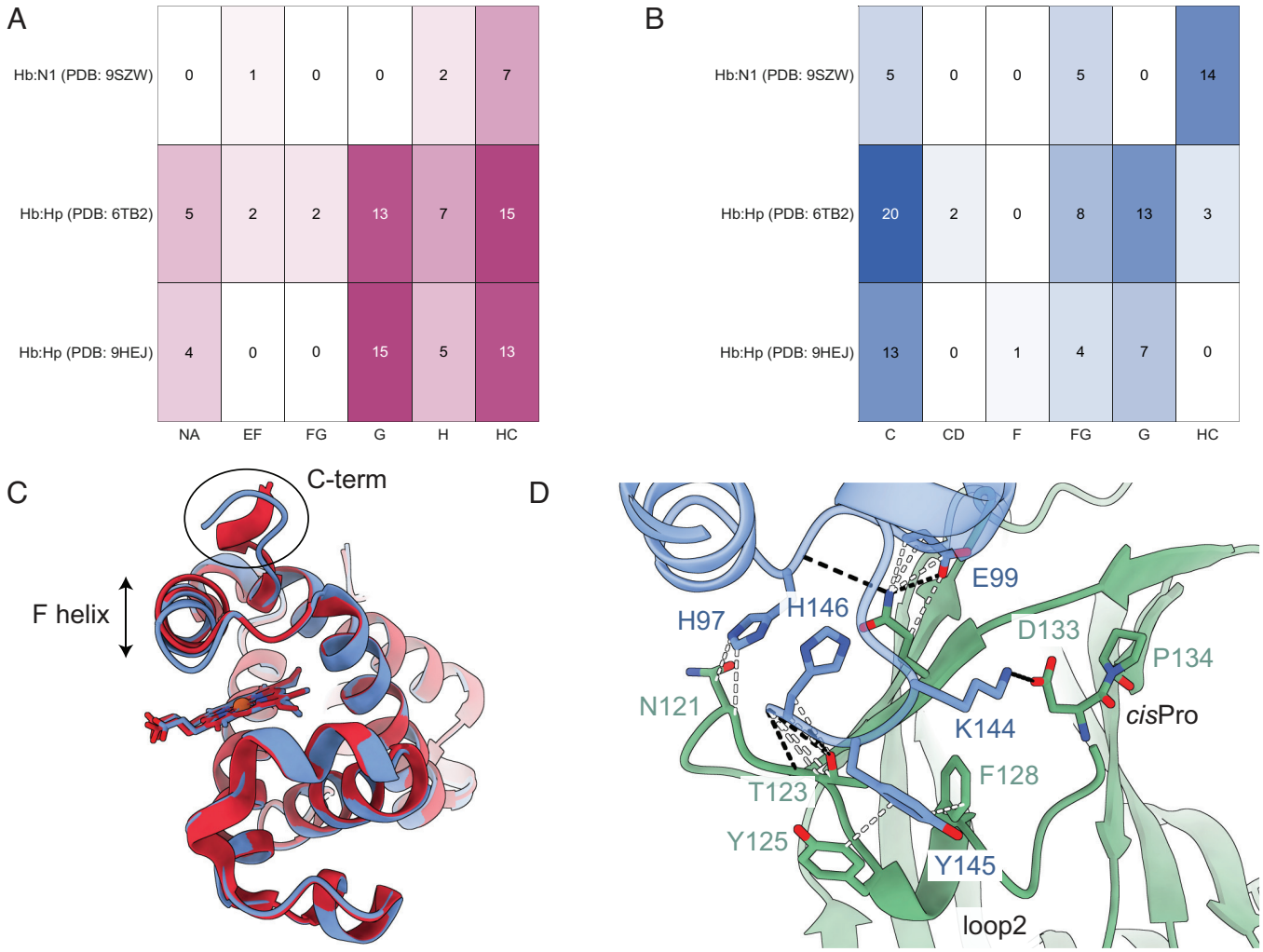


Fig. 2. Contact profiles and structural basis of $IsdH^{N1}$ recognition of Hb. (*A* and *B*) Heatmap of polar and nonpolar contacts between Hb and either N1 (PBD ID 9SZW) or Hp [PDB ID 9HEJ (31) and 6TB2 (15)] for α- (*A*) and β-chains (*B*) identified using RING and mapped onto Hb secondary structure elements. Numbers within the cells indicate the number of contacts detected for each segment pair. Labels on the x-axis follow the classical Hb secondary structure nomenclature, where helices are indicated by letters (e.g., C, G) and connecting loops are denoted by the adjacent helix names (e.g., NA indicates the N-terminal–helix A loop, FG the loop between helices F and G). (*C*) Structural superposition of the β-Hb chains from the cryo-EM $1IsdH:Hb_{dim}$ model (light blue) and the reference structure [PDB ID 2DN1 (33), red]. (*D*) Structural details of the interaction between $IsdH^{N1}$ and the β-chains of Hb. The region encompassing loop2 of NEAT1 (shown in green) forms multiple contacts with the β-chain (light blue), involving residues within the FG loop and the C-terminal region. These interactions likely contribute to the stabilization of loop2 in its folded conformation.

Downloaded from https://www.pnas.org by UNIVERSITA DEGLI STUDI DI PARMA on May 11, 2026 from IP address 160.78.140.1.

Table 2. Binding free energy (ΔG) and dissociation constants (K_D) of the complexes estimated using PRODIGY (34)

Protein–protein complex	ΔG (kcal mol^{-1})	K_D (μM)
NEAT1:Hb_{dim}	−10.2	0.034
NEAT1:α-Hb	−7.6	2.7
Hp:Hb_{dim}	−14.4	2.9×10^{-5}

Protein–protein complexes analyzed were NEAT1 binding at the Hb dimer–dimer interface (NEAT1:Hb_{dim}, PDB 9SZW), NEAT1 binding to the α subunit of Hb [NEAT1:α-Hb, PDB ID 3SKZ (30)], and Hp binding at the dimer–dimer interface of Hb [Hp:Hb_{dim}, PDB ID 9HEJ (31)].

superposition, the Cα RMSD between the two dimers was 1.26 Å, indicating an overall good alignment. However, visual inspection revealed the most pronounced deviation in the β-chain F helix, which appears closer to the heme in our cryo-EM model, leading to a partial closure of the heme-binding pocket relative to the reference. This rearrangement seems to result from a concerted movement of helix H and the β-chain C-terminal segment—previously identified as part of the NEAT1 interaction surface (Fig. 2 *A* and *B*)—and could play a key role in stabilizing or destabilizing this helical element, which is critical for heme extraction by hemophores (16, 29). A final observation regarding the NEAT1 domain from the cryo-EM model concerns loop2, which in NEAT1 spans residues 125 to 129, whose structure is a known signature of Hb-binding in both IsdH and IsdB. Loop2 adopts a 3_{10} helix structure upon binding to Hb, guided by a hydrophobic pattern within the A and E helices (36). This folding was further correlated with the *cis–trans* isomerization of the proline located five residues downstream of loop2, corresponding to Pro134 in NEAT1, which stabilizes the ordered conformation (29). In our cryo-EM model, loop2 is largely solvent-exposed, yet forms the 3_{10} helix, with Pro134 in the *cis* conformation (Fig. 2*D*). Notably, upstream residues (120 to 124) of the loop2 itself, and downstream residues engage contacts with the Hb β-chain, including the FG loop and C-terminal region. The stabilization of *cis*-Pro134 through contacts involving residues flanking loop2 indicates that the isomerization event likely precedes and enables loop2 ordering. Thus, at least in this context, the formation of *cis*-Pro134 appears to be the causal step that promotes the emergence of the loop2 3_{10} helix, even in a solvent-exposed environment.

Mechanistic Insights into Early and Late Stages of Full-Length IsdH Binding to Hb. The binding mode described in the previous section was likely driven by the interaction of the NEAT2-Linker2-NEAT3 segment with the α-chains of Hb. If NEAT2-Linker2-NEAT3 had instead bound the β-chains, the NEAT1 domain would have been positioned over the α-chains, as previously reported in the literature (23, 30). To explore the potential α/β-chain selectivity of individual IsdH fragments, two constructs were employed: the isolated $IsdH^{N1}$ domain and the $IsdH^{N2L}$ segment. These constructs were used in pull-down assays with isolated Hb chains (*SI Appendix*, Fig. S5 *B* and *C*). The results revealed a clear preference of $IsdH^{N1}$ for the α-chains (*SI Appendix*, Fig. S5*B*), whereas $IsdH^{N2L}$ appeared capable of interacting also with the β-chains (*SI Appendix*, Fig. S5*C*). Therefore, the biochemical data alone cannot fully account for the binding mode of IsdH in complex with Hb, pointing to underlying structural determinants that shape its interaction mechanism. Indeed, our model of the IsdH:Hb complex revealed that the NEAT3 domain, responsible for heme extraction, is rigidly positioned near the heme-binding pocket of Hb. This sharply contrasts with the high flexibility previously observed for NEAT3 using the truncated $IsdH^{N2N3}$ construct (18). However, this flexibility was observed in a model in which two NEAT2-Linker2-NEAT3 fragments bound an Hb dimer, whereas in the present structure only one Hb chain is occupied by NEAT2-Linker2-NEAT3 and NEAT1 binds the Hb dimer–dimer interface. It is therefore reasonable that the cryo-EM complex containing two NEAT2-Linker2-NEAT3 units per Hb dimer represents a later stage of the interaction, while the structure reported here likely captures an early stage of the binding process. Similarly, it is plausible that IsdH interacts with metHb to form the 2IsdH:Hb_{dim} complex (i.e., two hemophores bound to an Hb dimer) to maximize heme extraction. Consistent with this hypothesis, SEC-LS confirmed that IsdH associates with metHb under conditions ensuring two IsdH molecules per metHb dimer (*SI Appendix*, Fig. S6 and Table S4), which is distinct from the stoichiometry previously reported for the IsdH:oxyHb complex. These results suggest the interpretation that efficient heme extraction is associated with this higher-order assembly. To further investigate whether the change in stoichiometry arises from altered affinity, we compared the binding of IsdH to oxyHb and metHb using ELISA (Fig. 3*A*). The measurements, performed with immobilized IsdH, yielded K_D of 57.0 ± 10.1 nM for oxyHb and 62.0 ± 16.0 nM for metHb, indicating that the oxidation state of the heme iron does not measurably affect the overall affinity. Therefore, the observed difference in complex stoichiometry between IsdH:oxyHb and IsdH:metHb complexes arises not from changes in binding strength but rather from structural constraints that permit 2IsdH:Hb_{dim} complex formation specifically with metHb.

Functional and Kinetic Characterization of IsdH:metHb Complexes. To investigate heme extraction, we monitored spectroscopically heme transfer by evaluating the characteristic shift in the Soret region that reflects heme movement from the Hb pocket to that of IsdH (17, 18). The reaction was monitored by time-resolved optical absorbance (TR-OA) using a stopped-flow apparatus equipped with a photodiode array (PDA) detector. At the stoichiometry identified for the IsdH:oxyHb complex (1IsdH:Hb_{dim}; 1.5 μM IsdH and 1.5 μM metHb dimer), no appreciable spectral changes were observed (*SI Appendix*, Fig. S7*A*), indicating that heme transfer did not occur. Increasing the concentration of IsdH in solution (3 μM, 7.5 μM, and 15 μM) progressively enhanced the spectral features characteristic of heme extraction and transfer (*SI Appendix*, Fig. S7 *B–D*). These kinetic results are fully consistent with the mechanistic model proposed above, indicating that efficient heme extraction by IsdH is associated with the formation of a 2IsdH:Hb_{dim} complex with metHb. In line with this interpretation, the only previous study using full-length IsdH reported heme transfer only under a 20-fold molar excess of IsdH (27), a condition compatible with the need to populate such higher-order assemblies. To dissect the kinetic process in greater detail, the trace for TR-OA of the IsdH–metHb reaction was first preprocessed using singular value decomposition (SVD, *SI Appendix*, Fig. S7*E*), and the kinetic profile of the first component (the only one considered relevant for probing heme extraction, *SI Appendix*, Fig. S7*F*) was analyzed. In addition, the reaction was monitored by recording the intrinsic tryptophan fluorescence of IsdH under identical experimental conditions. Indeed, fluorescence has previously been used to probe hemophore binding to Hb (18, 37). TR-OA and Time-Resolved Fluorescence (TR-F) traces were fitted using the Maximum Entropy Method (MEM, *SI Appendix*, Fig. S7*G*), following Sottini et al. (38). This model-independent approach was essential for handling data spanning a wide range of IsdH-to-Hb ratios, from stoichiometric (1IsdH:Hb_{dim}) to near pseudo-first-order conditions (up to 10 IsdH molecules per Hb dimer), which were

Downloaded from https://www.pnas.org by UNIVERSITA DEGLI STUDI DI PARMA on May 11, 2026 from IP address 160.78.140.1.

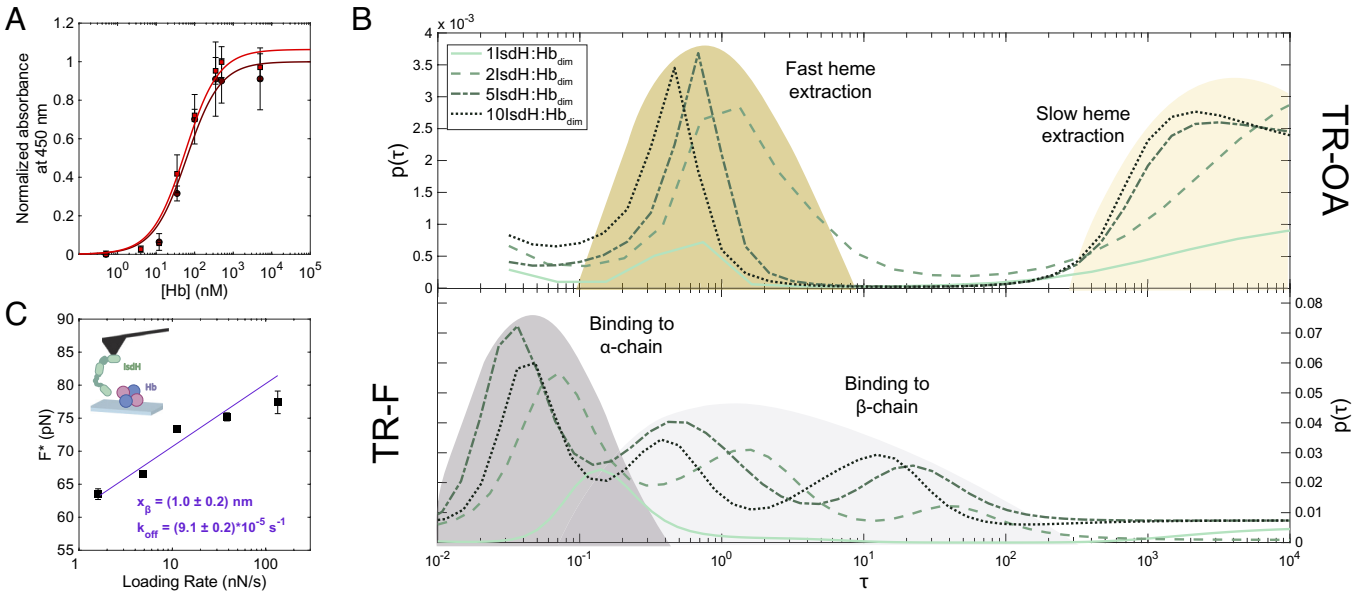


Fig. 3. IsdH–Hb interaction in the context of heme acquisition. (*A*) Binding affinities of IsdH for oxyHb (red) and metHb (brown). (*B*) Lifetime distributions [p(τ)] as a function of relaxation times (τ) obtained from MEM fitting of TR-OA (*Top*) and TR-F (*Bottom*) traces at four IsdH concentrations (metHb fixed at 1.5 μM, dimer concentration; 1.5 μM = 1IsdH:Hb$_{dim}$, 3 μM = 2IsdH:Hb$_{dim}$, 7.5 μM = 5IsdH:Hb$_{dim}$, 15 μM = 10IsdH:Hb$_{dim}$ stoichiometric ratios). In the TR-OA traces, dark and light-yellow shaded areas highlight the two heme-extraction processes. In the TR-F traces, light and dark gray shaded areas indicate the binding of IsdH to the α- and β-subunits, respectively. (*C*) Bell-Evans plot showing the most probable unbinding force (F*) as a function of the logarithm of the loading rate for the IsdH:metHb complex. The purple line represents the linear fit based on the Bell-Evans model (Eq. **4**; R^2 = 0.79). Experiments were performed in triplicate (n = 3).

otherwise difficult to reconcile with a single kinetic model. Unlike multiexponential fitting, which requires a predefined number of kinetic components, MEM yields a continuous distribution of relaxation times, thereby revealing distinct kinetic processes without imposing a specific functional form (Fig. 3*B*). In the TR-OA data, two kinetic phases became clearly visible only at IsdH concentrations sufficient to yield at least two molecules per Hb dimer, while no significant spectral changes were observed at the 1IsdH:Hb$_{dim}$ stoichiometry. These two kinetic phases display comparable amplitudes and together account for the full magnitude of the observed spectral change. This behavior is consistent with two distinct processes equally contributing to heme extraction, potentially associated with the two globin chains of Hb; however, individual kinetic components could not be unambiguously assigned. While only the initial phase of the very slow process was captured during the 300 s stopped-flow measurement, monitoring with a conventional spectrophotometer over a prolonged period demonstrated that approximately 40 min were required for full completion (*SI Appendix*, Fig. S8 *A* and *B*). Interestingly, as the concentration of IsdH increases, both kinetic populations show a decrease in their characteristic relaxation times (τ), indicating that the processes accelerate. This behavior is fully consistent with classical kinetic concepts, where increasing the reagent concentration enhances the rate of the extraction process. Similarly, fluorescence measurements revealed distinct kinetic processes. In the simplest case, at 1IsdH:Hb$_{dim}$ stoichiometry, a single process is observed, most plausibly reflecting binding to the α-chains. As the concentration of IsdH increases, the kinetic profile becomes more complex, revealing three distinct relaxations. The fastest phase corresponds to the process already detected using a 1IsdH:Hb$_{dim}$ ratio, whereas the two slower ones likely represent sequential steps related to the interaction of IsdH with the β-chains. The intermediate one is kinetically coupled to the fast heme extraction phase detected by TR-OA, consistent with the onset of heme release occurring upon binding of the second hemophore to the Hb dimer. The slowest process likely reflects a subsequent step within the same binding pathway, possibly corresponding to the completion of the second IsdH–Hb interaction or a conformational rearrangement in the 2IsdH:Hb$_{dim}$ complex. All three kinetic phases accelerate with increasing IsdH concentration, consistent with their dependence on free IsdH in solution. The relatively slow heme extraction kinetics observed for IsdH alone prompted us to investigate whether the presence of IsdB could enhance this process. To this end, we analyzed the rate of heme extraction from metHb using the two purified proteins (*SI Appendix*, Fig. S8 *C* and *D*). Under these conditions, the process reached near completion within ~5 min. In contrast, IsdB alone, under the same conditions, exhibited a substantially reduced transition amplitude (*SI Appendix*, Fig. S8 *E* and *F*). These observations suggest that, if colocalized on the *S. aureus* surface, IsdH and IsdB may simultaneously engage different globin chains (α and β, respectively) of the same Hb dimer, thereby jointly enhancing heme extraction.

Mechanical Characterization of the IsdH:metHb Interaction by Atomic Force Spectroscopy. Atomic Force Spectroscopy (AFS) was then employed to investigate the mechanical aspects of the interaction (Fig. 3*C*). In this approach, a microscopic cantilever tip is functionalized with IsdH and brought into contact with metHb immobilized on a surface. As the tip retracts, the forces required to detach the protein from its binding partner are measured, providing quantitative insight into the strength and mechanics of the interaction. This method has been successfully applied to study IsdB and the IsdH^{N2N3} fragment in earlier studies (18, 39). The most probable unbinding force (F*) was measured as a function of the logarithm of the loading rate (LR) (Fig. 3*C*), revealing a linear relationship across the analyzed range (2 to 200 nN/s), consistent with the Bell–Evans model (40, 41). This behavior, typical of slip bonds, indicates that increasing applied force facilitates dissociation, in contrast to catch bonds, where force stabilizes the interaction (42, 43). Such slip-bond behavior is characteristic of most protein–protein interactions, reflecting the general tendency of these complexes to weaken under mechanical stress. Fitting the unbinding forces

Downloaded from https://www.pnas.org by UNIVERSITA DEGLI STUDI DI PARMA on May 11, 2026 from IP address 160.78.140.1.

across the range of loading rates to the Bell–Evans model yielded a dissociation rate constant (k_{off}) of (9.1 ± 0.2) × 10^{-5} s^{-1} and a width of the energy barrier along the direction of the applied force (x_β) of 1.0 ± 0.2 nm, consistent with typical noncovalent biomolecular interactions (44). These results agree with previous data obtained for the $IsdH^{N2N3}$ fragment (18), indicating that, at the mechanical level, the full-length and the minimal functional constructs behave similarly when interacting with metHb. Interestingly, the dissociation rate constant measured for IsdH indicates a significantly longer resident time compared to IsdB [k_{off} = (2.2 ± 0.4) × 10^{-2} s^{-1} (39)]. This highlights distinct mechanical properties of IsdH and IsdB in their interaction with Hb, with IsdH forming a more persistent complex and IsdB exhibiting catch bond-like behavior (39). Catch bonds are characteristic of certain proteins, such as adhesins, which are able to strengthen their interaction under mechanical stress. When identified in the IsdB–metHb interaction, it was hypothesized that this mechanism could help stabilize the complex with the human protein in environments where mechanical forces might otherwise disrupt it, such as in the bloodstream. By reinforcing the bond under stress, the protein remains bound for sufficient time to complete heme extraction. Notably, the complex dissociation rate constant reported for IsdB corresponds to lifetimes in the order of tens of seconds, which are comparable to the timescale required for heme removal from Hb. A structural determinant underlying catch bond-like behavior has been proposed to involve a proline isomerization within the Hb-binding domain, stabilized by surrounding residues in IsdB (45). This feature may enable the force-induced conformational transitions responsible for catch bond behavior. In contrast, such stabilization has not been demonstrated for the $IsdH^{N2N3}$ fragment (18), consistent with the absence of catch bond-like behavior. The present results extend this observation to IsdH. Overall, these findings indicate that IsdB and IsdH adopt distinct mechanical strategies: IsdB exploits force-enhanced binding to sustain interaction under mechanical stress, whereas IsdH achieves stability mediated by multiple binding domains, independent of applied force.

Discussion

We reported a structural and kinetic analysis providing a comprehensive view of how full-length *S. aureus* IsdH engages Hb and orchestrates heme extraction when it is freely available in the extracellular environment. The cryo-EM structure of the IsdH:HbCO complex reveals that the initial binding event primarily involves the Hb α-chains, leading to the formation of a compact 1IsdH:Hb_{dim} complex in which IsdH engages a single Hb dimer. Remarkably, this study also provides direct structural evidence of NEAT1 binding at the dimer–dimer interface of Hb—a previously unrecognized interaction that may play a key role in promoting Hb dimer destabilization and positioning the receptor for subsequent steps of the extraction process. Upon oxidation of oxyHb to metHb, IsdH can form the 2IsdH:Hb_{dim} complex, an assembly that correlates with heme transfer. However, our kinetic analysis indicates that, despite being able to complete extraction, this process is intrinsically inefficient. The reaction exhibits a clearly biphasic profile, with an initial rapid phase followed by a second step that is orders of magnitude slower. As a result, heme extraction by IsdH alone occurs on a timescale dramatically longer than that observed for IsdB. Strikingly, this limitation is overcome in the presence of IsdB, as heme extraction within the 1IsdB:1IsdH:Hb_{dim} complex proceeds with kinetics comparable to those of IsdB alone. Our data support the emergence of two distinct functional modes of action for IsdH (Fig. 4), with the versatility of NEAT1 playing a central role. Indeed, NEAT1 can bind Hb in two distinct ways: through the interaction at the dimer–dimer interface and through the canonical pose involving the A–E helices of the Hb α-chain. When free Hb is available in solution, this versatility in binding geometry likely increases the efficiency with which NEAT1 captures Hb and delivers it to downstream domains. The long, flexible Linker1 connecting NEAT1 to NEAT2 likely facilitates this role, acting as a molecular "fishing line" that enables NEAT1 to capture additional Hb dimers and funnel them toward the bacterial surface. At this stage, the colocalization of IsdH with IsdB enables rapid and efficient heme extraction, reconciling the high-affinity Hb binding properties of IsdH with its intrinsically slow extraction kinetics and supporting a cooperative model for iron acquisition.

A distinct scenario emerges in the context of the Hb:Hp complex. Here, Hp occupies the Hb dimer–dimer interface, while the NEAT2–NEAT3 region of IsdH engages the α-chains, as observed in our model with Hb alone. In this configuration, NEAT1 is unlikely to access the Hb dimer and may instead exploit the long flexible Linker1 to reach and bind the α-chains of the second Hb dimer associated with the opposite Hp protomer. In this configuration, IsdB, which has been reported not to interact with Hb:Hp (16), would not contribute to heme extraction. Instead, IsdH alone may mediate Hb engagement and efficiently extract heme, as demonstrated in previous studies (15, 26). In addition, it likely interferes with CD163 recognition by simultaneously engaging both Hb dimers, as previously suggested (26).

Future studies should address how the full-length Hb receptor interacts with the Hb:Hp complex and mediate heme extraction. Although available structural data obtained with the minimal functional construct [PDB ID 6TB2 (15)] suggests that heme removal may occur preferentially from β-chains, our results highlight how the use of the full-length receptor may reveal additional and more complex mechanisms, warranting targeted biochemical and structural investigations. Ultimately, this work provides an integrated framework for understanding how full-length IsdH coordinates substrate binding, mechanical engagement, and heme transfer, thereby expanding our comprehension of iron acquisition strategies in *S. aureus* and setting the stage for rational efforts to inhibit this essential heme extraction pathway.

Materials and Methods

Protein Production and Purification. IsdH (UniProt ID Q8NW39, residues 86 to 665) and $IsdH^{N1}$ (UniProt ID Q8NW39, residues 86 to 232) were cloned into the pASK-IBA3plus® vector (IBA Lifesciences) to express a C-terminal Strep-tag®II fusion protein in *E. coli*. Transformed cells were grown on LB agar with 100 μg/mL ampicillin, and a single colony was used to inoculate LB broth (100 μg/mL ampicillin) overnight at 37 °C with shaking. The cultures were diluted 1:100 into fresh medium and grown to mid-log phase (OD_{600} ≈ 0.8), followed by induction with 0.2 μg/mL anhydrotetracycline for 3 h at 37 °C. Cells were harvested by centrifugation and washed with PBS. Cell pellets were resuspended in lysis buffer (Buffer W: 100 mM Tris pH 8.0, 150 mM NaCl, 1 mM EDTA, supplemented with lysozyme and protease inhibitors) and disrupted by sonication. After centrifugation to remove debris, the supernatant was loaded onto a Strep-Tactin® XT affinity column, and IsdH was eluted with BXT buffer (IBA Lifesciences). To obtain the apo form, heme was removed by extraction with methyl ethyl ketone (MEK) following previously published protocols (46). The protein solution was acidified to pH 2.0 and extracted with prechilled MEK (1:1 volume) to remove heme. After phase separation, the aqueous layer containing apo-protein was collected, neutralized with pH 8.0 buffer to allow refolding, and dialyzed to remove residual MEK. A final size-exclusion chromatography (SEC) step using a XK 16/600 column (GE Healthcare) packed *in-house* with Superdex 200 prep grade resin was performed to eliminate aggregates. The resulting apo-protein

Downloaded from https://www.pnas.org by UNIVERSITA DEGLI STUDI DI PARMA on May 11, 2026 from IP address 160.78.140.1.

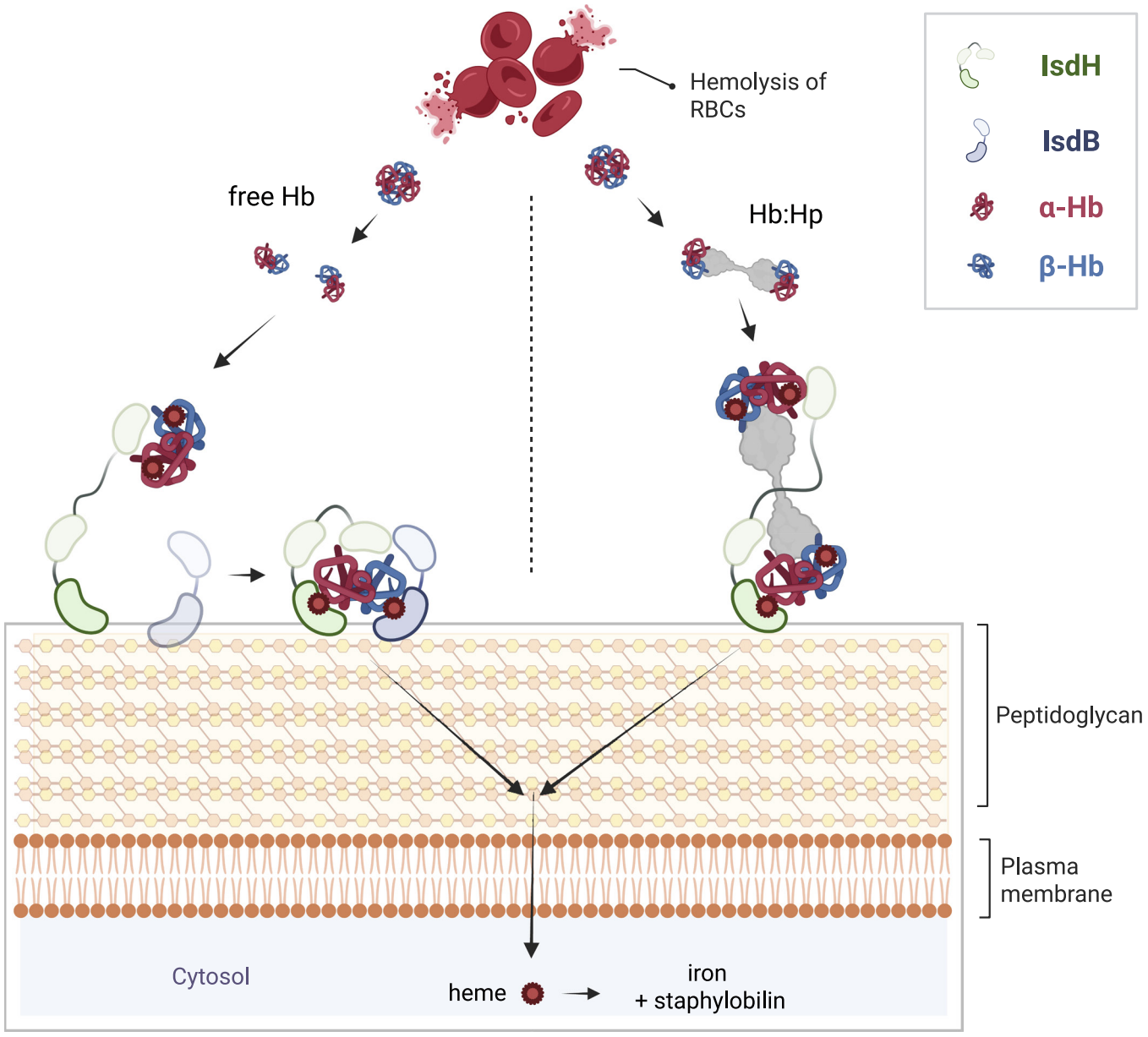


Fig. 4. Dual modes of IsdH-mediated heme acquisition under hemolytic conditions. Schematic model illustrating two physiological scenarios in which IsdH contributes to heme extraction from Hb. *Left*, under conditions of extensive hemolysis, Hp becomes saturated (28), leading to the accumulation of free Hb dimers in the extracellular milieu. In this context, the flexible NEAT1 domain of IsdH, connected via Linker 1, may function as a "fishing line" to capture Hb and recruit it toward the bacterial surface. However, our data indicate that the presence of IsdH alone, even at high molar excess (*SI Appendix*, Fig. S8) is insufficient to support rapid and productive heme extraction. Instead, efficient heme acquisition likely requires cooperation with IsdB. In our structural model, the NEAT2–NEAT3 domains of IsdH engage the α-subunits of Hb, leaving the β-subunits accessible for IsdB, which has been reported to preferentially bind β-chains (29). This coordinated arrangement enables optimal heme extraction when both receptors are present, consistent with our observation that efficient heme extraction occurs in the presence of one IsdH and one IsdB molecule per Hb dimer (*SI Appendix*, Fig. S8). *Right*, in an alternative and well-established scenario, a fraction of Hb released during hemolysis is sequestered by Hp, forming Hb:Hp complexes. Under these conditions, IsdH plays a primary role, as it is capable of directly binding the Hb:Hp complex and extracting heme (15, 26). Following extraction, heme is transferred across the cell wall and membrane, ultimately reaching the cytosol, where it is used as it is or degraded to release iron. Created in BioRender. De Bei (2026) https://BioRender.com/y733yeo.

was >95% pure, aliquoted, flash-frozen in liquid nitrogen, and stored at −80 °C. IsdH^{N2L} (UniProt ID Q8NW39, residues 326 to 543) was produced through deletion of the heme binding domain, as previously described in Buoli Comani et al. (18). IsdB (UniProt ID Q8NX66, residues 125 to 485) was codon-optimized for *E. coli* and cloned into pASK-IBA3plus to generate a C-terminal Strep-tag® II construct. Transformed *E. coli* cells were grown to mid-log phase (OD600 0.5 to 0.6) in M9 medium at 37 °C and induced with anhydrotetracycline (0.2 μg/mL) for 20 h at 20 °C. Cells were harvested, lysed by sonication in buffer W (100 mM Tris pH 8, 150 mM NaCl, 1 mM EDTA) supplemented with lysozyme and protease inhibitors, and clarified by centrifugation. The protein was purified using Strep-Tactin®XT affinity chromatography and eluted with biotin, followed by size-exclusion chromatography (Superdex 75) in buffer W to remove high-molecular-weight contaminants, as previously described (29). Human hemoglobin A (Hb) was purified from outdated blood units obtained from nonsmoking volunteers, from whom written informed consent was obtained, at a certified blood transfusion center. All samples were deidentified by the transfusion center prior to their release for research use, and no identifiable personal information was accessible to the investigators. The study was conducted in accordance with Italian law on blood donation and usage (Italian law 219/2005) and following the protocol reported by De Bei et al. (37). Red blood cells were isolated by centrifugation, lysed by osmotic shock, and Hb was separated from cellular debris by high-speed centrifugation. The protein was then purified by cation-exchange chromatography on a CM-Sephadex C-50 column using a linear pH gradient, and its concentration and oxidation state were assessed by visible absorption spectroscopy. MetHb was generated by oxidation of the heme group with 5 mM

Downloaded from https://www.pnas.org by UNIVERSITA DEGLI STUDI DI PARMA on May 11, 2026 from IP address 160.78.140.1.

potassium ferricyanide $K_3[Fe(CN)_6]$ (Fluka) and the oxidizing agent was removed using a Sephadex G-25 desalting column. Carboxyhemoglobin (HbCO) was prepared by equilibrating an oxyhemoglobin (oxyHb) solution with a stream of pure carbon monoxide at 4 °C. The isolation of native α- and β-Hb subunits was performed as previously described in our previous work (18). In brief, HbCO was incubated with p-chloromercuribenzoate (CMB) in 20 mM potassium phosphate buffer (pH 7.0), using an eightfold molar excess of CMB relative to Hb. The ionic strength was adjusted to 0.1 M with potassium chloride, and the pH was subsequently lowered to 6.0. The reaction mixture was incubated overnight at 4 °C. Following incubation, the sample was equilibrated in separation buffer 1 (10 mM potassium phosphate, pH 5.8) and loaded onto a CM-Sephadex column. The α- and β-subunits were separated using a pH gradient ranging from 5.8 to 7.8, generated by progressively increasing the proportion of separation buffer 2 (10 mM potassium phosphate, pH 8.6) using an ÄKTA Prime FPLC system. Under these conditions, β-chains eluted at approximately pH 6.4, whereas α-chains eluted at pH values above 7.4. After chromatographic separation, CMB was removed by treatment with cysteine, using a 50-fold molar excess relative to the thiol groups to be restored. Finally, the purified subunits were buffer-exchanged into the Hb storage buffer.

Size-Exclusion Chromatography. SEC experiments were performed at 25 °C using an Agilent 1260 HPLC system (Agilent Technologies, Santa Clara, CA) equipped with a Zenix-C SEC-300 column (3 μm, 4.6 × 150 mm; Sepax Technologies), a Diode Array Detector, a Refractive Index Detector and a Dual-Angle Light Scattering Detector. The column was equilibrated with PBS (pH 7.4) and operated at a constant flow rate of 0.35 mL/min. Protein samples were injected at ~1 g/L (see Fig. 1 and *SI Appendix*, Fig. S6 for exact concentrations). The system was calibrated with bovine serum albumin (BSA, ~10 g/L), and the LS detector was used to estimate MWs.

Enzyme-Linked ImmunoSorbent Assay (ELISA). Hemophore–Hb affinities were determined using an optimized ELISA protocol previously established in Cozzi et al. (47), and Buoli Comani et al. (18). Briefly, Strep-tagged IsdH was immobilized on Strep-Tactin®XT microplates (IBA Lifesciences) and incubated with increasing concentrations of Hb (0.5 nM to 5 μM). Bound complexes were detected with HRP-conjugated anti-Hb polyclonal antibodies (Abcam) at 1:10,000 dilution and quantified by absorbance change at 450 nm due to 3,3′,5,5′-tetramethylbenzidine (TMB, Acros Organics) oxidation. All incubations were carried out at 4 °C. Data were normalized and fitted to a single-site binding isotherm (Eq. **1**) to determine the dissociation constant (K_D):

$$A_{450nm} = \frac{A_{max} \times [\mathrm{Hb}]}{K_D + [\mathrm{Hb}]}. \qquad [\mathbf{1}]$$

Cryo-EM Specimen Preparation and Data Collection. Following a previously validated approach (18, 29), HbCO, which is resistant to heme extraction, was used to capture the pre-extraction complex with IsdH. IsdH was mixed with HbCO to yield one IsdH molecule per Hb dimer, to a final concentration of 6 g/L in 10 mM HEPES, 1 mM EDTA, pH 7.2. 3-([3-cholamidopropyl]dimethylammonio)-2-hydroxy-1-propanesulfonate (CHAPSO) was added to 8 mM immediately before plunge freezing to minimize preferred particle orientation. Aliquots (3 μL) were applied to glow-discharged R1.2/1.3 QUANTIFOIL® grids, blotted for 3 s, and vitrified in liquid ethane using a Vitrobot Mark IV at 4 °C and 99% humidity. Data were collected at the School of Biological Sciences Cryo-EM Facility, University of Cambridge, on a Titan Krios (Thermo Fisher Scientific) operated at 300 kV and equipped with an F4i counting direct detector and a SelectrisX energy filter (Thermo Fisher Scientific) set to a 10-eV slit width. Automated data acquisition was performed using EPU (Thermo Fisher Scientific) at 165,000× magnification (0.729 Å/pixel). A total of 4,752 micrographs were acquired with a defocus range of –0.6 to –1.8 μm.

Cryo-EM Data Processing. Single-particle analysis of the IsdH:HbCO complex was performed in RELION 5.0 (48). Micrographs were preprocessed following the standard SPA workflow, including beam-induced motion correction and CTF estimation. Particle autopicking was carried out using the TOPAZ neural network (49), yielding a total of 654,333 particles that were extracted for further processing. Successive rounds of 2D and 3D classification enabled the separation of two distinct structural populations of the complex (*SI Appendix*, Fig. S2).

Protein Structure Prediction, Modeling and Analysis. The atomic model of the 1IsdH:Hb_{dim} complex was generated using Namdinator (50), starting from a composite model built from two crystallographic structures: the $IsdH^{N2N3}$:Hb complex (PDB ID 9SZW) and the isolated $IsdH^{N1}$ domain (PDB ID 3SZK). The resulting model was manually adjusted and refined using ISOLDE (51). For the 1IsdH:2Hb_{dim} complex, Namdinator (50) was used directly without further manual refinement. To investigate the contact network within the 1IsdH:Hb_{dim} complex, RING (52) was employed via its online server (https://ring.biocomputingup.it/), allowing systematic identification and analysis of residue–residue interactions between IsdH and Hb. The structures of full-length IsdH in complex with Hb at different stoichiometries were predicted using AlphaFold3 (53) via the online AlphaFold Server (https://alphafoldserver.com/) using the default parameters. Binding affinities (ΔG and K_D) of protein–protein complexes were estimated using PRODIGY (54), available at https://wenmr.science.uu.nl/prodigy/.

Kinetic Characterization of Heme Extraction. Kinetic measurements were performed on an SX20 stopped-flow spectrometer (Applied Photophysics, UK), following a previously described method (18, 37). All experiments were carried out at 20 °C in PBS, pH 7.4. The reactions were initiated by rapidly mixing metHb (1.5 μM, calculated on the dimeric concentration) with different concentrations of IsdH (corresponding to the following stoichiometries): 1.5 μM (1IsdH:Hb_{dim}), 3 μM (2IsdH:Hb_{dim}), 7.5 μM (5IsdH:Hb_{dim}), and 15 μM (10IsdH:Hb_{dim}). The instrument (dead time ≈ 1.5 ms) was equipped with a 150 W xenon arc lamp and operated either in absorbance mode (TR-OA)–coupled to a Direct Coupled Photodiode Array (PDA) detector–or in fluorescence mode (TR-F), using a photomultiplier tube for detection. TR-OA kinetics were recorded as 1,000-point datasets acquired in triplicate, whereas TR-F traces comprised 10,000 points collected in duplicate. In both cases, data were acquired over 300 s with logarithmic time spacing. TR-OA datasets were analyzed by Singular Value Decomposition (SVD) to identify the main spectral and temporal components. For each measurement, the absorbance matrix (dimensions n x m, where n corresponds to the number of wavelengths and m to the number of time delays) was converted into difference spectra relative to the first delay. All such matrices from different experiments were concatenated along the time dimension, yielding a single global matrix (n x Σm), which was then subjected to SVD. In this way, the U-matrix (spectral basis vectors) was common to all datasets, while the V-matrices (temporal components) were re-extracted separately for each individual experiment. The V vectors from replicate datasets were averaged, and only the relevant components–based on spectral interpretability and kinetic significance–were selected for further analysis. Replicate TR-F traces were averaged prior to further analysis, ensuring consistent signal-to-noise ratios and reproducibility across kinetic series. The averaged kinetic data, TR-OA (selected SVD components) and TR-F, were analyzed using a custom MATLAB routine developed in-house, following the Maximum Entropy Method (MEM) described by Sottini et al. (38). The algorithm uses the conceptual framework of the MemExp approach (55) but was entirely reimplemented in MATLAB [MATLAB. (2025). *Version R2025a*. Natick, Massachusetts: The MathWorks Inc.] to allow flexible control over regularization and model composition. In brief, the experimental kinetics I(t) were modeled as the sum of M discrete exponential components and a continuous distribution of relaxation times, p(τ), regularized by an entropy term (Eq. **2**):

$$I(t) \approx \sum_{k=1}^{M} A_k e^{-t/\tau_k} + \int p(\log\tau)\, e^{-t/\tau}\, d(\log\tau). \qquad [\mathbf{2}]$$

The fitting procedure minimizes the objective function (Eq. **3**):

$$F = \frac{1}{2} \sum_i [I(t_i) - I_{\mathrm{fit}}(t_i)]^2 + \alpha \sum_j p_j \log\left(\frac{p_j}{m_j}\right). \qquad [\mathbf{3}]$$

where the first term represents the least-squares residuals and the second enforces maximum entropy regularization with respect to a uniform prior m. The regularization weight α controls the balance between data fidelity and smoothness of p(τ). Optimization was performed using MATLAB's constrained minimization routine (fmincon), with additional options for baseline estimation and adaptive logarithmic sampling of the relaxation-time grid. The resulting discrete amplitudes (A^k, τ^k) and continuous distributions p(τ) were then used to reconstruct the fitted traces (I_{fit}) and to describe the overall kinetic heterogeneity of the system.

Downloaded from https://www.pnas.org by UNIVERSITA DEGLI STUDI DI PARMA on May 11, 2026 from IP address 160.78.140.1.

Heme extraction experiments were carried out in PBS (pH 7.4) at 20 °C using a Cary 4000 UV–Vis spectrophotometer (Agilent). Spectra were collected from 350 nm to 700 nm, monitoring heme transfer at 406 nm. Following Gianquinto et al. (56), 1.5 μM metHb (per Hb dimer) was preincubated for 3 min before initiating the reaction by adding IsdH (15 μM, 10-fold excess), IsdH and IsdB (1.5 μM each) or IsdB (1.5 μM).

Pull-Down Assay With Isolated Hb α- and β-Chains. To assess the binding specificity of $IsdH^{N1}$ and $IsdH^{N2L}$ toward individual Hb chains, pull-down assays were performed using MagStrep® Strep-Tactin® magnetic beads (IBA Lifesciences). Beads were washed once with Buffer W, and 30 μL of StrepTag-II–tagged purified protein was added and incubated for 10 min at room temperature to ensure immobilization. After removal of unbound protein, 30 μL of the Hb α/β mixture (36 μM each, heme concentration) was added and incubated under the same conditions. Bound proteins were eluted with 100 μL BXT buffer, and the eluates were analyzed by SDS–PAGE (15% acrylamide-bisacrylamide, 29:1 solution) to evaluate the interaction profile of $IsdH^{N1}$ and $IsdH^{N2L}$ with each globin chain.

Atomic Force Spectroscopy (AFS) Functionalization and Measurements. The covalent immobilization of IsdH and metHb on AFM tip and glass substrates, respectively, was performed by following previously established protocols (39, 45). Briefly, silicon nitride AFM tips (cantilever D, SNL-10; Bruker Corporation, MA) with a nominal spring constant of 0.06 N/m were incubated with 2% (v/v) 3-mercaptopropyl-trimethoxysilane (MPTMS; Sigma-Aldrich) in toluene (99.5%; Sigma-Aldrich) for thiol activation. Successively, the tips were reacted for 3 h with 1 mM N-hydroxysuccinimide–polyethylene glycol–maleimide (NHS–PEG–MAL, 3.4 kDa; Iris Biotech) dissolved in DMSO (99.9%; Sigma-Aldrich). Functionalization with IsdH was then performed by overnight incubation at 4 °C with 25 μL of 5 μM protein in Buffer W, allowing covalent coupling between NHS esters of the PEG and lysine residues on the protein surface. For the substrate, aldehyde-functionalized glass slides (1 cm^2; PolyAn GmbH, Germany) were exposed to 50 μL of 10 μM metHb (heme concentration) in Buffer W for 4 h at 25 °C in air to promote covalent attachment between aldehyde and protein amino groups. After functionalization, both tips and substrates were thoroughly rinsed with buffer and Milli-Q water, and residual reactive sites were passivated by incubation for 30 min in 1 M ethanolamine hydrochloride (pH 8.5) in Milli-Q water (GE Healthcare). Substrates were used immediately after substrate functionalization, while IsdH-functionalized tips were stored in Buffer W at 4 °C to preserve protein activity. AFS experiments were conducted at room temperature using a Nanoscope IIIa/Multimode AFM (Veeco Instruments, NY) operated in liquid mode with Buffer W saturated with nitrogen to maintain the oxidation state of metHb. Force curves were collected by approaching the IsdH functionalized tip to metHb-charged substrate and then retracting from it. The approach was terminated upon reaching a maximum contact force of 0.7 nN, with a ramp size of 150 nm and an encounter time of 100 ms. The approach velocity was fixed at 50 nm/s, whereas the retraction velocity varied between 50 and 4,200 nm/s to vary the loading rate (LR), given by the product of the cantilever retraction velocity (v) and the effective spring constant of the system (k_{syst}); the latter being determined from the slope of the retraction curve immediately before the unbinding event (57). The unbinding force was obtained by multiplying the measured cantilever deflection by its effective spring constant (k_{eff}), experimentally determined according to the procedure in Kienberger et al. (58). Curves characterized, during the retraction phase, by sharp peaks with starting and ending points at zero deflection line, and by a nonlinear curved shape before the jump-off, which was related to the stretching features of the PEG linker, were selected as related to specific unbinding events according to the procedure reported in (44, 59). For each loading rate, approximately 1,000 force–distance curves were collected, using the same functionalized cantilever; the histograms of the unbinding forces are shown in *SI Appendix*, Fig. S9. All measurements were repeated in triplicate to ensure reproducibility. To investigate the force dependence of bond dissociation, the most probable unbinding force (F*) was plotted against the natural logarithm of the loading rate (r). The resulting data were analyzed according to the Bell–Evans model (40, 41), which describes how the application of an external force lowers the energy barrier for dissociation, thereby accelerating bond rupture. According to this model, F* and the loading rate are related through the following expression (Eq. **4**):

$$F^* = \frac{k_B T}{x_\beta} ln\left(\frac{r x_\beta}{k_{off} k_B T}\right). \quad [4]$$

where k_B is the Boltzmann constant, T the absolute temperature, k_{off} the dissociation rate constant in the absence of applied force, and x_β the width of the energy barrier along the force direction. Blocking assays were performed to verify the specificity of the molecular interaction by acquiring force–distance curves at a retraction velocity of 350 nm/s using an IsdH-functionalized cantilever preincubated with a 10 μM Hb solution (*SI Appendix*, Fig. S9). Measurements were then conducted against the Hb-coated substrate in Buffer W at 25 °C.

Data, Materials, and Software Availability. The dataset generated in this study has been deposited in the Figshare database under accession code (https://figshare.com/10.6084/m9.figshare.30751553) (60). The 3D cryo-EM density maps generated in this study have been deposited in the Electron Microscopy Data Bank (EMDB) under accession codes EMD-55389 (61) and EMD-55478 (62) and the atomic coordinates have been deposited in the Protein Data Bank, with accession code 9SZW (63).

ACKNOWLEDGMENTS. This project was funded by "PRIN-2020–Defeat antimicrobial resistance through iron starvation in *Staphylococcus aureus* (ERASE)" (Grant 2020AE3LTA) to S.B. and A.R.B. This research benefits from the High-Performance Computing facility of the University of Parma, Italy (https://www.hpc.unipr.it). This work has been carried out in the frame of the ALIFAR project, funded by the Italian Ministry of University through the program "Dipartimenti di Eccellenza 2023–2027." V.B.C. received cryo-EM training through Wellcome/MRC funded program (218785/Z/19/Z) and Advanced kinetics training through MOSBRI (ESC4: Advanced kinetics approaches to unravel protein structure and function). O.D.B. received cryo-EM training through Wellcome Trust and MRC funded Cryo-EM Training Program (Advanced Single Particle Cryo-EM Course, 2025). B.F.L. is supported by Wellcome Trust investigator award (222451/Z/21/Z).

Author affiliations: [a]Department of Food and Drug, University of Parma, Parma 43124, Italy; [b]Interdepartmental Center Biopharmanet-TEC, University of Parma, Parma 43124, Italy; [c]Department of Medicine and Surgery, University of Parma, Parma 43125, Italy; [d]Department of Biochemistry, University of Cambridge, Cambridge CB2 1GA, United Kingdom; [e]Biophysics and Nanoscience Centre, Department of Ecological and Biological Sciences, Università della Tuscia, Viterbo 01100, Italy; and [f]Institute of Biophysics, National Research Council, Pisa 56124, Italy

1. S. Y. C. Tong, J. S. Davis, E. Eichenberger, T. L. Holland, V. G. Fowler, Staphylococcus aureus infections: Epidemiology, pathophysiology, clinical manifestations, and management. *Clin. Microbiol. Rev.* **28**, 603–661 (2015).
2. A. R. Richardson, G. A. Somerville, A. L. Sonenshein, Regulating the intersection of metabolism and pathogenesis in Gram-positive bacteria. *Microbiol. Spectr.* **3**, 3.3.11 (2015).
3. G. A. Somerville, R. A. Proctor, At the crossroads of bacterial metabolism and virulence factor synthesis in Staphylococci. *Microbiol. Mol. Biol. Rev.* **73**, 233–248 (2009).
4. C. C. Murdoch, E. P. Skaar, Nutritional immunity: The battle for nutrient metals at the host–pathogen interface. *Nat. Rev. Microbiol.* **20**, 657–670 (2022).
5. J. C. Grigg, G. Ukpabi, C. F. M. Gaudin, M. E. P. Murphy, Structural biology of heme binding in the *Staphylococcus aureus* Isd system. *J. Inorg. Biochem.* **104**, 341–348 (2010).
6. M. Marchetti *et al.*, Iron metabolism at the interface between host and pathogen: From nutritional immunity to antibacterial development. *Int. J. Mol. Sci.* **21**, 2145 (2020).
7. P.-Y. Chen, E. P. Skaar, Heme in bacterial pathogenesis and as an antimicrobial target. *Chem. Rev.* **125**, 11120–11144 (2025).
8. S. K. Mazmanian *et al.*, Passage of heme-iron across the envelope of *Staphylococcus aureus*. *Science* **1979**, 906–909 (2003).
9. A. G. Cheng *et al.*, Genetic requirements for *Staphylococcus aureus* abscess formation and persistence in host tissues. *FASEB J.* **23**, 3393–3404 (2009).
10. H. K. Kim *et al.*, IsdA and IsdB antibodies protect mice against *Staphylococcus aureus* abscess formation and lethal challenge. *Vaccine* **28**, 6382–6392 (2010).
11. A. Dryla, D. Gelbmann, A. Von Gabain, E. Nagy, Identification of a novel iron regulated staphylococcal surface protein with haptoglobin-haemoglobin binding activity. *Mol. Microbiol.* **49**, 37–53 (2003).
12. R. M. Pilpa *et al.*, Functionally distinct NEAT (NEAr transporter) domains within the *staphylococcus aureus* IsdH/HarA protein extract heme from methemoglobin. *J. Biol. Chem.* **284**, 1166–1176 (2009).
13. C. B. F. Andersen *et al.*, Haptoglobin. *Antioxid. Redox Signal.* **26**, 814–831 (2017).
14. K. L. Sædorup *et al.*, The *Staphylococcus aureus* protein IsdH inhibits host hemoglobin scavenging to promote heme acquisition by the pathogen. *J. Biol. Chem.* **291**, 23989–23998 (2016).

Downloaded from https://www.pnas.org by UNIVERSITA DEGLI STUDI DI PARMA on May 11, 2026 from IP address 160.78.140.1.

15. J. H. Mikkelsen, K. Runager, C. B. F. Andersen, The human protein haptoglobin inhibits IsdH-mediated heme-sequestering by *Staphylococcus aureus*. *J. Biol. Chem.* **295**, 1781–1791 (2020).
16. C. F. M. Bowden *et al.*, Structure–function analyses reveal key features in *Staphylococcus aureus* IsdB-associated unfolding of the heme-binding pocket of human hemoglobin. *J. Biol. Chem.* **293**, 177–190 (2018).
17. M. Sjodt *et al.*, Energetics underlying hemin extraction from human hemoglobin by *Staphylococcus aureus*. *J. Biol. Chem.* **293**, 6942–6957 (2018).
18. V. Buoli Comani *et al.*, Hemoglobin receptor redundancy in *Staphylococcus aureus*: Molecular flexibility as a determinant of divergent hemophore activity. *J. Struct. Biol. X* **12**, 100138 (2025).
19. K. Ellis-Guardiola *et al.*, The *Staphylococcus aureus* IsdH receptor forms a dynamic complex with human hemoglobin that triggers heme release via two distinct hot spots. *J. Mol. Biol.* **432**, 1064–1082 (2020).
20. C. F. M. Gaudin, J. C. Grigg, A. L. Arrieta, M. E. P. Murphy, Unique heme-iron coordination by the hemoglobin receptor IsdB of *Staphylococcus aureus*. *Biochemistry* **50**, 5443–5452 (2011).
21. M. Watanabe *et al.*, Structural basis for multimeric heme complexation through a specific protein-heme interaction: The case of the third NEAT domain of IsdH from *Staphylococcus aureus*. *J. Biol. Chem.* **283**, 28649–28659 (2008).
22. C. F. Dickson *et al.*, Structure of the hemoglobin-isdh complex reveals the molecular basis of iron capture by *Staphylococcus aureus*. *J, Biol. Chem.* **289**, 6728–6738 (2014).
23. C. F. Dickson, D. A. Jacques, R. T. Clubb, J. M. Guss, D. A. Gell, The structure of haemoglobin bound to the haemoglobin receptor IsdH from *Staphylococcus aureus* shows disruption of the native α-globin haem pocket. *Acta Crystallogr. D Biol. Crystallogr.* **71**, 1295–1306 (2015).
24. T. Spirig *et al.*, Staphylococcus aureus uses a novel multidomain receptor to break apart human hemoglobin and steal its heme. *J. Biol. Chem.* **288**, 1065–1078 (2013).
25. A. Dryla *et al.*, High-affinity binding of the staphylococcal HarA protein to haptoglobin and hemoglobin involves a domain with an antiparallel eight-stranded β-barrel fold. *J. Bacteriol.* **189**, 254–264 (2007).
26. K. L. Sæderup *et al.*, The *Staphylococcus aureus* protein IsdH inhibits host hemoglobin scavenging to promote heme acquisition by the pathogen. *J. Biol. Chem.* **291**, 23989–23998 (2016).
27. S. Valenciano-Bellido *et al.*, Structure and role of the linker domain of the iron surface-determinant protein IsdH in heme transportation in *Staphylococcus aureus*. *J. Biol. Chem.* **298**, 101995 (2022).
28. D. J. Schaer, P. W. Buehler, A. I. Alayash, J. D. Belcher, G. M. Vercellotti, Hemolysis and free hemoglobin revisited: Exploring hemoglobin and hemin scavengers as a novel class of therapeutic proteins. *Blood* **121**, 1276–1284 (2013).
29. O. De Bei *et al.*, Cryo-EM structures of staphylococcal IsdB bound to human hemoglobin reveal the process of heme extraction. *Proc. Natl. Acad. Sci. U.S.A.* **119**, e2116708119 (2022).
30. K. K. Kumar *et al.*, Structural basis for hemoglobin capture by *Staphylococcus aureus* cell-surface protein. IsdH. *J. Biol. Chem.* **286**, 38439–38447 (2011).
31. R. X. Zhou, M. K. Higgins, Scavenger receptor CD163 multimerises to allow uptake of diverse ligands. *Nat. Commun.* **16**, 6623 (2025).
32. The Croonian Lecture, 1968–The haemoglobin molecule. *Proc. R. Soc. Lond. B Biol. Sci.* **173**, 113–140 (1969).
33. S.-Y. Park, T. Yokoyama, N. Shibayama, Y. Shiro, J. R. H. Tame, 1.25 Å resolution crystal structures of human haemoglobin in the oxy, deoxy and carbonmonoxy forms. *J. Mol. Biol.* **360**, 690–701 (2006).
34. L. C. Xue, J. P. Rodrigues, P. L. Kastritis, A. M. Bonvin, A. Vangone, PRODIGY: A web server for predicting the binding affinity of protein–protein complexes. *Bioinformatics* **32**, 3676–3678 (2016).
35. M. J. Nielsen *et al.*, Haptoglobin-related protein is a high-affinity hemoglobin-binding plasma protein. *Blood* **108**, 2846–2849 (2006).
36. B. A. Fonner *et al.*, Solution structure and molecular determinants of hemoglobin binding of the first NEAT domain of *IsdB* in *Staphylococcus aureus*. *Biochemistry* **53**, 3922–3933 (2014).
37. O. De Bei *et al.*, Time-resolved x-ray solution scattering unveils the events leading to hemoglobin heme capture by staphylococcal IsdB. *Nat. Commun.* **16**, 1361 (2025).
38. S. Sottini, S. Abbruzzetti, C. Viappiani, L. Ronda, A. Mozzarelli, Determination of microscopic rate constants for CO binding and migration in myoglobin encapsulated in silica gels. *J. Phys. Chem. B* **109**, 19523–19528 (2005).
39. V. Botti *et al.*, Nanoscale dynamical investigation of the hemoglobin complex with the bacterial protein IsdB: Is their interaction stabilized by catch bonds? *Nanoscale* **16**, 4308–4316 (2024).
40. G. I. Bell, Models for the specific adhesion of cells to cells. *Science* **1979**, 618–627 (1978).
41. E. Evans, Probing the relation between force–lifetime–and chemistry in single molecular bonds. *Annu. Rev. Biophys. Biomol. Struct.* **30**, 105–128 (2001).
42. B. T. Marshall *et al.*, Direct observation of catch bonds involving cell-adhesion molecules. *Nature* **423**, 190–193 (2003).
43. W. Thomas, Catch bonds in adhesion. *Annu. Rev. Biomed. Eng.* **10**, 39–57 (2008).
44. A. R. Bizzarri, S. Cannistraro, The application of atomic force spectroscopy to the study of biological complexes undergoing a biorecognition process. *Chem. Soc. Rev.* **39**, 734–749 (2010).
45. F. Pancrazi *et al.*, Proline isomerization modulates the bacterial *IsdB*/hemoglobin interaction: An atomic force spectroscopy study. *Discover Nano* **20**, 20 (2025).
46. K. Ellis-Guardiola, J. Soule, R. T. Clubb, Methods for the extraction of heme prosthetic groups from hemoproteins. *Bio. Protoc.* **11**, e4156 (2021).
47. M. Cozzi *et al.*, Identification of small molecules affecting the interaction between human hemoglobin and *Staphylococcus aureus* IsdB hemophore. *Sci. Rep.* **14**, 8272 (2024).
48. S. H. W. Scheres, RELION: Implementation of a Bayesian approach to cryo-EM structure determination. *J. Struct. Biol.* **180**, 519–530 (2012).
49. T. Bepler *et al.*, Positive-unlabeled convolutional neural networks for particle picking in cryo-electron micrographs. *Nat. Methods* **16**, 1153–1160 (2019).
50. R. T. Kidmose *et al.*, Namdinator – automatic molecular dynamics flexible fitting of structural models into cryo-EM and crystallography experimental maps. *IUCrJ* **6**, 526–531 (2019).
51. T. I. Croll, Isolde: A physically realistic environment for model building into low-resolution electron-density maps. *Acta Crystallogr. D Struct. Biol.* **74**, 519–530 (2018).
52. A. Del Conte *et al.*, RING 4.0: Faster residue interaction networks with novel interaction types across over 35, 000 different chemical structures. *Nucleic Acids Res.* **52**, W306–W312 (2024).
53. J. Abramson *et al.*, Accurate structure prediction of biomolecular interactions with AlphaFold 3. *Nature* **630**, 493–500 (2024).
54. R. V. Honorato *et al.*, Structural biology in the clouds: The WeNMR-EOSC ecosystem. *Front. Mol. Biosci.* **8**, 729513 (2021).
55. P. J. Steinbach, Filtering artifacts from lifetime distributions when maximizing entropy using a bootstrapped model. *Anal. Biochem.* **427**, 102–105 (2012).
56. E. Gianquinto *et al.*, Interaction of human hemoglobin and semi-hemoglobins with the *Staphylococcus aureus* hemophore IsdB: A kinetic and mechanistic insight. *Sci. Rep.* **9**, 18629 (2019).
57. J. L. Hutter, J. Bechhoefer, Calibration of atomic-force microscope tips. *Rev. Sci. Instru.* **64**, 1868–1873 (1993).
58. F. Kienberger, A. Ebner, H. J. Gruber, P. Hinterdorfer, Molecular recognition imaging and force spectroscopy of single biomolecules. *Acc. Chem. Res.* **39**, 29–36 (2006).
59. M. Liu *et al.*, Direct hemin transfer from IsdA to IsdC in the iron-regulated surface determinant (Isd) heme acquisition system of *Staphylococcus aureus*. *J. Biol. Chem.* **283**, 6668–6676 (2008).
60. V. Buoli Comani *et al.*, Raw data "Refining the mechanism of heme acquisition from free hemoglobin by *Staphylococcus aureus* IsdH." FigShare. https://figshare.com/10.6084/m9.figshare.30751553. Deposited 11 February 2026.
61. V. B. Comani, O. De Bei, B. F. Luisi, S. Bettati, Human carboxyhemoglobin bound to full-length *Staphylococcus aureus* IsdH - IsdH:Hbdim complex. EMDB. https://www.ebi.ac.uk/emdb/EMD-55389. Deposited 11 October 2025.
62. V. B. Comani, O. De Bei, B. F. Luisi, S. Bettati, Human carboxyhemoglobin bound to full-length *Staphylococcus aureus* IsdH - 1IsdH:2Hbdim complex. EMDB. https://www.ebi.ac.uk/emdb/EMD-55478. Deposited 24 October 2025.
63. V. B. Comani, O. De Bei, B. F. Luisi, S. Bettati, Human carboxyhemoglobin bound to full-length *Staphylococcus aureus* IsdH - IsdH:Hbdim complex. PDB. https://doi.org/10.2210/pdb9szw/pdb. Deposited 11 October 2025.

Downloaded from https://www.pnas.org by UNIVERSITA DEGLI STUDI DI PARMA on May 11, 2026 from IP address 160.78.140.1.